

N77-14651

Tmx 71244

X-695-76-255

PREPRINT  
(REVISED)

# TERRESTRIAL KILOMETRIC RADIATION: 3 - AVERAGE SPECTRAL PROPERTIES

(NASA-TM-X-71244) TERRESTRIAL KILOMETRIC  
RADIATION: 3-AVERAGE SPECTRAL PROPERTIES  
(NASA) 27 p HC A03/MF A01 CSCL 04A

N77-14651

30

Unclas  
G3/46 58321

MICHAEL L. KAISER  
JOSEPH K. ALEXANDER

NOVEMBER 1976



————— **GODDARD SPACE FLIGHT CENTER** —————  
**GREENBELT, MARYLAND**

**For information concerning availability  
of this document contact:**

**Technical Information Division, Code 250  
Goddard Space Flight Center  
Greenbelt, Maryland 20771**

**(Telephone 301-982-4488)**

**"This paper presents the views of the author(s), and does not necessarily  
reflect the views of the Goddard Space Flight Center, or NASA."**

TERRESTRIAL KILOMETRIC RADIATION:  
3 - AVERAGE SPECTRAL PROPERTIES

Michael L. Kaiser and Joseph K. Alexander  
Planetary Sciences Branch  
Laboratory for Extraterrestrial Physics  
NASA/Goddard Space Flight Center  
Greenbelt, Maryland 20771

ABSTRACT

We present a study of the spectral properties of terrestrial kilometric radiation (TKR) derived from observations made by the Goddard radio astronomy experiments onboard the IMP-6 and RAE-2 spacecraft. As viewed from near the equatorial plane, TKR is most intense and most often observed in the 21-24 hr local time zone and is rarely seen in the 09-12 hr zone. The absolute flux levels in the 100-600 kHz TKR band increase significantly with increasing substorm activity as inferred from the auroral electrojet index (AE). In the late evening sector, the median power increases by about three orders of magnitude between quiet periods (AE < 75 $\gamma$ ) and disturbed periods (AE > 200 $\gamma$ ). The peak flux density usually occurs near 250 kHz, although the frequency of the peak in the flux spectrum appears to vary inversely with AE from a maximum near 300 kHz during very quiet times to a minimum below 200 kHz during very disturbed times. The half-power bandwidth is typically 100% of the peak frequency. The variation of TKR flux density with apparent source altitude indicates that source strength decreases more rapidly than  $R^{-2}$ .

## TKR 3: Average Spectral Properties

### INTRODUCTION

Satellite-borne measurements conducted in the past several years have shown that the radio spectrum near 300 kHz is often dominated by intense bursts of terrestrial kilometric radiation (TKR) which originate in the magnetosphere. A number of workers have demonstrated that TKR is associated with various manifestations of magnetospheric substorms such as the auroral electrojet index AE (Dunckel et al., 1970; Voots et al., 1977), discrete auroral arcs (Gurnett, 1974) and particle precipitation patterns (Kaiser and Stone, 1975). Initial source location studies showed that the most intense emissions apparently originate from low altitudes in the evening sector in a region at, or near, auroral zone latitudes (Gurnett, 1974; Kurth et al., 1975; Kaiser and Stone, 1975). In earlier papers in this series we presented the results of a survey of the average two-dimensional source position distribution obtained from lunar orbit which showed that TKR was sometimes observed at large radial distances both in the evening sector near the plasma sheet (Alexander and Kaiser, 1976; hereinafter called paper 1) and also in the region of the dayside cusp and high latitude magnetosheath (Alexander and Kaiser, 1977; hereinafter called paper 2). In this paper we present a summary of the variations of spectral properties of TKR with source altitude, observer's local time, and substorm activity as measured by the AE index.

Earlier investigations of the spectral properties of TKR were often limited by relatively coarse frequency resolution or were confined to discussion of a few isolated, but "typical", events. Dunckel et al. (1970) noted that the emission possessed a low frequency cut-off of  $\sim 40$  kHz and that very high flux densities ( $\geq 10^{-14}$  W m<sup>-2</sup> Hz<sup>-1</sup>) were common at frequencies up to at least 100 kHz. The typical spectrum of a TKR event was described by Brown (1973) and illustrated by Gurnett (1974, 1975) and Kaiser and Stone (1975) to have a spectral peak between 100 and 500 kHz and a bandwidth of a few hundred kHz. In the present study we have used absolute flux measurements obtained from IMP-6 over a 525 day period with a frequency resolution of 5 channels/octave to determine how both the received power and spectrum of TKR change with AE and with the observer's location in the magnetosphere. Wherever possible, we have supplemented and confirmed the IMP-6 findings with similar, although less precise, flux measurements obtained from the RAE-2 spacecraft in lunar orbit. (Such comparisons are necessarily statistical since the IMP-6 experiment failed in September, 1972 after 19 months of operation and RAE-2 was not launched until June, 1973). We have used the two-dimensional source location measurements from the RAE-2 data reported in papers 1 and 2 to study the variation of observed flux with projected source altitude.

When one examines the dynamic spectra of individual TKR events in detail it becomes obvious that the spectral characteristics are often extremely complex. Indeed as we will illustrate, there is considerable evidence for fine structure in the dynamic spectra such as

variations of center frequency and bandwidth by up to  $\sim 50\%$ , drifting spectral features, and multiple spectral peaks all on a time scale of tens of minutes and less. In the present paper, however, we direct our attention primarily to a survey of the gross spectral properties of TKR since this broader view of the emission spectrum is important in order to begin to build and test a realistic theoretical explanation for the emission by providing a background or reference point against which individual detailed events may be compared.

#### INSTRUMENTATION

The primary source of absolute flux measurements used in this study has been the Goddard Space Flight Center radio astronomy experiment on the IMP-6 satellite (Explorer-43). This experiment consisted of a pair of step-frequency, 32-channel, total power radiometers connected to a 91-m electric dipole antenna situated in the satellite spin plane. One receiver covered the frequency range 30 kHz to 9.9 MHz with a 10 kHz pre-detection bandwidth and a post-detection integration time constant of 6ms, and the second receiver covered the frequency range 30 kHz to 4.9 MHz with a 3 kHz pre-detection bandwidth and a post-detection integration time constant of 40 ms. Each receiver made a full frequency scan every 5.11 sec. There were a total of 15 separate frequency channels in the decade frequency band 90 kHz to 900 kHz of interest for observations of TKR. Each receiver had a total dynamic range of 60 dB which was divided into two 30-dB ranges in order to provide an amplitude resolution of  $\pm 3\%$ . Based on periodic inflight noise calibration measurements, the total receiver gain drift during the 18-month experiment

lifetime was only 1.5 dB. Details of the receiver calibration have been presented by Brown (1973).

The RAE-2 receivers (described in paper 1) are nearly identical to their IMP-6 counterparts, but we have used the IMP-6 data as the basic source of absolute flux spectra measurements for several reasons. First, compared to the RAE-2 receivers the IMP-6 receivers had a wider useable dynamic range and better performance with respect to unwanted preamplifier intermodulation products (by  $\sim 10$  dB). Furthermore, the simple dipole antenna on IMP-6 was much more amenable to absolute power measurements than the relatively complex travelling-wave V-antennas on RAE-2. The RAE-2 data, on the other hand, provided somewhat better statistical coverage in local time and had the unique capability of providing two-dimensional source position information from lunar occultations.

The IMP-6 satellite was launched on March 13, 1971, into a highly elliptical orbit (eccentricity  $\sim 0.94$ , apogee  $> 200,000$  km) inclined  $28^\circ$  to the equator. The orbital period of 4.15 days coupled with a very low precession rate meant that each successive apogee occurred 16 minutes earlier in sub-satellite local time than the preceding apogee. During the lifetime of the Goddard IMP-6 radio astronomy experiment, the sub-satellite point at apogee was always in the Northern magnetic hemisphere with an overall average sub-satellite geomagnetic latitude of  $+17^\circ \pm 2^\circ$  for times when IMP-6 was above  $25 R_E$  (50% of each orbit). In this study, we used data from the time of full antenna extension on April 20, 1971, until the experiment failed on September 26, 1972, -

a span of 525 days. The RAE-2 data used in papers 1 and 2 were also used in this study. These RAE-2 data consisted of approximately 260 individual lunar occultations of TKR events recorded between July 1973 and July 1975. For each of these measurements, the apparent location of TKR source regions was deduced from occultation immersion-emersion timings as discussed in papers 1 and 2. The average power level from before and after an occultation was used to characterize the flux from a given source region.

## OBSERVATIONS

### Spectra

TKR power flux density spectra were obtained from the IMP-6 data as a function of AE and observer's local time in the following manner. First, in order to reduce uncertainties in the measured flux level arising from uncertainties in the precise distance of the satellite to the source; we used only those data obtained from beyond  $25 R_E$  so that the source distance would always be large compared to the distance uncertainty. The individual flux values were normalized to a constant distance of  $25 R_E$  by multiplying by  $(R/25R_E)^2$ . Second, the data were examined to determine if TKR activity was being detected, and those periods with no TKR were excluded from the analysis. We defined TKR to be present when three or more channels in the band from 92 kHz through 600 kHz simultaneously exhibited flux levels 5 dB or more above background. At frequencies above  $\sim 200$  kHz, background corresponded to cosmic background as determined by Brown (1973). Below 200 kHz, background corresponded to the average spectrum associated with Brown's

"LF" component which is probably the same as Gurnett's (1975) "continuum" emission. The background level was above receiver threshold at all frequencies using these criteria. TKR was not detected in only 10% of the data collected from above  $25 R_E$ , and nearly all of these cases corresponded to observations made from above the dayside hemisphere.

Finally, the data satisfying both the distance and TKR threshold criteria were sorted for each observing frequency into 2-dB flux density bins allowing us to form histograms of the number of samples as a function of flux density. We subdivided these flux density histograms for each observing frequency into 3-hour bins of sub-satellite local time, and the individual samples in each local time sector were categorized according to the value of the AE index at the time of the observation. Two representative histograms for 250 kHz (near the center of the TKR band) are shown in Figure 1. The number of samples in each flux density bin have been converted to probability (in percent) per unit flux interval by dividing by the total number of samples and the flux density bin size. The two flux density distributions shown correspond to a local time zone where TKR occurs infrequently (06-09 hr) and to the local time zone where TKR occurs most often (21-24 hr). In the 06-09 hr zone, only those data obtained when AE was very low ( $< 75\gamma$ ) are shown, whereas, for the 21-24 hr zone data obtained when AE was high ( $> 200\gamma$ ) are shown. The straight lines with their indicated slopes were determined from linear least squares fits. Other frequency channels in the 92-600 kHz band show similar slopes for these two LT-AE combinations. For other combinations, the flux distributions at 250 kHz

are intermediate between the two extremes shown in Figure 1.

The vast difference in the flux distributions between the morning and late evening sectors can be appreciated by comparison of probabilities over the same flux range. The probability of observing a burst with a flux density of  $10^{-18} \text{ W m}^{-2} \text{ Hz}^{-1}$  is approximately the same for both local time zones ( $\sim 1.5\%$ ). However, the probability of observing emission more powerful than  $10^{-18} \text{ W m}^{-2} \text{ Hz}^{-1}$  is nearly 93% for the 21-24 hr zone and only 2% for the 06-09 hr zone.

Signals above  $\sim 10^{-16} \text{ W m}^{-2} \text{ Hz}^{-1}$  saturate the IMP-6 receiver and are simply recorded as  $\sim 10^{-16} \text{ W m}^{-2} \text{ Hz}^{-1}$ ; thus, the apparent slope change near this limit in the 21-24 hr distribution may be an artifact. However, Gurnett's (1974) Figure 5, when converted to a probability distribution also indicates a steep slope for the most intense bursts. The sharp change in slope at the low flux end of the morning zone distribution is simply a result of observations being limited by cosmic background radiation.

We have determined the median power flux density from the histograms for each observing frequency for each local time and the results are shown in Figure 2. Each local time panel displays median power flux (adjusted for an observer at  $R = 25 R_E$ ) versus observing frequency. Within each panel are three spectra corresponding to magnetically quiet times ( $AE \leq 75$ ), moderately active periods ( $75 < AE < 200$ ), and disturbed periods ( $AE \geq 200$ ). (This particular division of the data with respect to AE provides essentially equal numbers of IMP-6 measurements in each AE class.) The overall low-latitude radiation

pattern of TKR with highest intensities in the late evening and a minimum in the mid-morning sectors is evident in Figure 2 independent of the value of AE. The flux increases abruptly between the 12-15 hr bin and the 15-18 hr bin and decreases before 06 hr in close agreement with the single frequency histogram of Figure 3 in paper 1.

Figure 2 shows that there is a direct relationship between TKR flux and AE at practically all local times. In the evening hemisphere, the median flux density increases by more than two orders of magnitude between quiet periods ( $AE < 75$ ) and disturbed periods ( $AE > 200$ ). The median flux at the peak of the spectrum for  $AE > 200$  conditions over the evening sector can only be estimated from our data because of receiver saturation effects. The arrows in the 18-21, 21-24, and 00-03 hour bins show the estimated lower limit to the median flux density in the spectral region affected by saturation level signals (flux density  $> 2 \times 10^{-16} \text{ W m}^{-2} \text{ Hz}^{-1}$ ). Gurnett (1974) showed events at 178 kHz with flux densities of  $\sim 10^{-14} \text{ W m}^{-2} \text{ Hz}^{-1}$  at the 1% occurrence level, thus the median flux levels during disturbed periods, particularly in the 21-24 hr zone, may be underestimated by  $\sim 10$  dB. For  $AE < 200$  and at other local times we do not expect the results in Figure 2 to be seriously affected by saturation events. Using an average beam width of 3.5 sr as derived by Green et al. (1977) at 178 kHz, and a bandwidth of  $\sim 200$  kHz, the median event in the 21-24 hr zone during disturbed times may amount to a total radiated power of  $\sim 3 \times 10^7 \text{ W}$ . Thus, Gurnett's (1974) estimate of events as powerful as  $10^9 \text{ W}$  seems to be realistic.

There is clear evidence of a variation of the frequency of the peak of the spectrum,  $f_o$ , with substorm activity. For example, for observations in the evening sectors between 18 hr and 03 hr the average  $f_o$  is  $\sim 300$  kHz for  $AE < 75$ . For periods of high AE in the same local time range we find  $f_o$  is close to 200 kHz.

The characteristic TKR spectral shape evident in the 15-03 hr hemisphere is not obvious in the 03-15 hr hemisphere. Although TKR events were most definitely seen when the spacecraft was above the 03-15 hr hemisphere, their occurrence rate was such that the median flux values probably represent a blend of TKR and Gurnett's (1975) continuum radiation. Plots of the average flux spectra (rather than median flux) for this local time range show spectral shapes similar to those in the late evening sector, but at much lower flux levels. At 210 kHz, the probability of observing a TKR event in the morning sector with flux between  $10^{-17}$  and  $10^{-16}$   $W m^{-2} Hz^{-1}$  is only  $\sim 1\%$  during disturbed periods compared with  $\sim 10\%$  probability in the evening sector. The low-intensity dayside source of emission described by Kaiser and Stone (1975) may also contribute to the spectral shape in the 03-15 hr hemisphere, although the "TKR" existence criterion (3 channels  $> 5$  dB above background) may have eliminated many of the observations of this source.

We have repeated the analyses described above and illustrated in Figure 2 using the average flux density rather than the median flux density for each AE and local time interval. Due to the relatively limited dynamic range of the IMP-6 receiver compared to the

wide dynamic range exhibited by TKR, it is necessary to delete intervals with intense saturation level TKR activity before calculating the average spectrum in the beam during disturbed periods so that artifacts arising from preamplifier intermodulation effects do not give a misleading picture of the spectral shape. Although the average spectra are therefore based on a somewhat smaller statistical sample, the results discussed above based on median flux densities are fully confirmed. We observe a clear direct relationship between average flux density and AE and an inverse relationship between AE and the frequency of the peak of the average flux spectrum.

It is apparent from Figure 2 that TKR exhibits a high-frequency cutoff between 600 and 800 kHz. In retrospect, the high-frequency cutoff of 1.7 MHz mentioned by Kaiser and Stone (1975) appears to have been caused by preamplifier intermodulation products during extremely intense events.

#### Altitude dependence

The variation of source flux with source altitude has been studied using RAE-2 data, and the results are illustrated in Figure 3. We have measured the geocentric distance to the projected source positions (at 292 kHz) for the occultation events of paper 1. The lower three panels of Figure 3 show the number of source regions in  $1-R_E$  geocentric distance increments for very intense (3b), moderate intensity (3c), and weak (3d) events. These events were all measured when the moon was within  $\pm 3$  hr of the dusk meridian plane (first quarter phase), so that the projection plane was approximately the noon-midnight

meridian plane. The intense events are concentrated near the earth with a mean distance of  $3.2 R_E \pm 1.8$ , whereas the weak events are rather uniformly scattered over a large projected radial distance range. In the top panel, we have determined the median flux of source regions occurring in  $2-R_E$  distance increments (0-2, 2-4, etc.) for all RAE-2 events (open circles) and for those viewed from near first quarter moon (filled circles). The point at  $1 R_E$  is a lower limit to the median flux because of the limited dynamic range of the RAE-2 receiver, whereas the values beyond  $10 R_E$  are weighted toward slightly higher flux because of the exclusion in papers 1 and 2 of TKR events less than 10 dB above galactic background. The three straight lines are drawn to show various slopes for the function  $S \propto R^\alpha$ . The "error" bars represent the size of each increment used in both flux density and radial distance. Although the placement of any single value in Figure 3a is somewhat arbitrary, it does seem clear that the slope is steeper than  $R^{-2}$ . Figure 3 clearly shows that the most intense TKR events seem to come from relatively low altitudes while those sources observed at large distances from the Earth are generally observed at weaker flux levels.

#### Specific examples

Although the spectra depicted in Figure 2 are typical of TKR activity in a statistical sense, they are certainly not representative of all events. We often observe TKR with "instantaneous" bandwidths less than those in Figure 2, and we observe peak flux frequencies ranging from 100 kHz to about 500 kHz. A substantial fraction of TKR

events appear to have two or more spectral peaks as if more than one source region were emitting simultaneously. In this section, we will illustrate the spectral complexity of TKR at the 10-min time resolution level. Figures 4 and 5 show the spectra associated with particular source regions as measured by RAE-2, while Figure 6 is an example of a dual-peaked event observed by IMP-6.

Figures 4 and 5 have a similar format. On the left of each panel is a diagram showing the orientation of the lunar occultation source position with respect to the Earth as seen from RAE-2 at the time of the observation. The coordinate system is described in paper 1 and is basically a modified version of the solar magnetic (SM) system with the Z axis parallel to the earth's dipole axis with the +Z direction always containing the pole tilted toward the sun. The +X direction (left) is toward the sun. The projection plane in each figure is approximately the noon-midnight meridian plane. Selected field lines from the MF73D geomagnetic field model of Mead and Fairfield (1975) have been superimposed on each diagram. The right half of each panel shows the flux spectrum (measured from  $60 R_E$ ) averaged over the 10-min intervals immediately preceding and following the occultation.

In Figure 4 we show two events where the emission appears to emanate from high latitudes above the night hemisphere. In Figure 4a, the spectrum peaks above 400 kHz, near the upper limit for the TKR peak frequency. The corresponding projected source region at 425 kHz is at a radial distance of  $\sim 3 R_E$  near  $70-75^\circ$  invariant latitude above the nighttime pole. In Figure 4b, apparently two source regions are

emitting simultaneously each associated with a slightly different spectral band. The high frequency source is located near the earth as typified by source position A at 250 kHz, whereas the more intense low-frequency source projects some  $4 R_E$  further from the earth at position B. Both sources seem to be "threaded" by the same field line near  $80^\circ$  invariant latitude, but their relative separation in altitude is much greater than any realistic model would predict for radiation generated near the electron plasma or gyro frequency at the apparent source locations.

In Figure 5, we show examples of spectra of TKR apparently associated with the magnetospheric cusp. In Figure 5a a low-intensity source with  $f_o \approx 300$  kHz is situated at a projected radial distance of  $6 R_E$  in the cusp region. In Figure 5b a considerably more intense event with  $f_o \approx 200$  kHz appears to emanate from a region near  $9 R_E$  at a latitude of about  $78^\circ$ .

Figure 5c represents an extreme example of emission from the magnetosheath near the cusp-magnetosheath interface region. The diagram on the left shows the approximate shape and orientation of the entire magnetosphere with a nominal magnetopause and bow shock indicated by solid lines. The dashed curves show the projections of the moon's limb as seen from RAE-2 at 0930 and 0940 UT. During this interval most of the magnetosphere was completely out of view, yet, as shown in the flux spectrum in the right-hand panel, a substantial amount of emission persists at frequencies below 210 kHz. This emission can emanate only from beyond the projected lunar limb which

would place it generally at or beyond the magnetopause.

Figure 6 illustrates the kind of dynamic complexity often observed in TKR activity. The upper left-hand panel shows the IMP-6 dynamic spectral data derived from ten-minute averages between 1300 and 2400 UT on August 30, 1972. TKR "storms" are observed in association with moderate substorm activity between 1300 and 1600 UT ( $AE \leq 200$ ) and between 1900 and 2200 ( $AE \leq 300$ ). Both events show evidence of a drift in the low frequency envelope of the emission from high ( $\geq 130$  kHz) to low ( $\leq 83$  kHz) within a period of the order of an hour. More remarkable is the obvious splitting of the dynamic spectrum of the second event into two distinct bands. This is illustrated in detail in the lower left-hand dynamic spectral plot with 5.1-sec time resolution and in the average flux spectrum shown on the right-hand side of the figure. Between 2010 and 2020 UT we find spectral peaks near 180 kHz and near 450 kHz. The ratio of the frequencies of the two spectral peaks varies between 2:1 and 3:1 during the period 1930 to 2130 UT. Some theoretical models of possible significance for TKR would predict harmonic structure in the emission (e.g.  $3f_g/2$ ,  $5f_g/2$ , etc., (Scarf, 1974)), but it is not yet clear whether this feature of the emission is due to frequency structure associated with a single source or with near simultaneous emission from multiple, spatially separated source regions.

#### DISCUSSION

The basic observational properties concerning the average behavior of the TKR flux spectrum can be summarized as follows:

1) The average power in the TKR band increases with increasing substorm activity as measured by AE.

2) The average  $f_o$  tends to decrease with increasing AE. The overall (i.e. all LT and all AE) average  $f_o$  is  $\approx 250$  kHz with a full width at half power of 200 kHz.

3) There is a relationship between flux and apparent source altitude such that the most intense events seem to occur close to the earth while the weaker events can be observed to emanate from a large altitude range. Additionally, as we first mentioned in paper 1, for a given event, low frequencies seem to emanate further from the earth than higher frequencies. This relationship holds for most of the 260 RAE-2 occultation events in this study. The distance distribution depicted in Figure 4 is fairly typical of this behavior. We have found no unambiguous cases where the lower frequencies appeared to emanate from closer to the earth than the higher frequencies.

4) The average power in the TKR band is much higher in the region from 15-06 hr local time than in the dayside region from 06-15 hr. The maximum flux is received in the 21-24 hr interval and the minimum flux in the 06-12 hr interval.

The flux versus altitude dependence imposes some restrictions on the type of mechanism necessary to explain the large altitude range of TKR sources. If the distant sources were the result of simple scattering from anomalously high density regions in the outer magnetosphere, then the observations shown in Figure 3 would require scattering efficiency to decrease with distance. However, the observation that

for a given TKR event successively lower frequencies emanate from increasingly higher altitudes is difficult to explain in terms of scattering from density anomalies. If radiation at a particular frequency were scattered by a density enhancement, we would expect all lower frequencies to also be scattered at the same point and we would expect the measured source positions to be independent of frequency. If the density anomaly were spatially large with a small density gradient, the measured source positions would appear progressively closer to the earth at successively lower frequencies, precisely opposite to the observations. On the other hand, we can not rule out the possibility of some form of wave-wave interaction which could result in preferential scattering of the TKR waves off plasma turbulence along selected field lines. The regions of intense plasma wave turbulence recently observed on auroral field lines by Gurnett and Frank (1976) may provide evidence that the conditions to support such a scattering mechanism can exist in the region of the magnetosphere from which TKR is often observed (Kennel, private communication, 1976).

In summary, the major observations of the TKR phenomena which have been discussed in this paper and papers 1 and 2 are the following:

- 1) The conditions necessary for TKR generation must be extremely commonplace since for observations taken from above the 21 to 24 hr local time sector we find occurrence probabilities in excess of 90% in the middle of the TKR spectral band.

- 2) TKR appears to be closely related to the spatial structure of the geomagnetic field as distorted by the interaction with the solar

wind. The source location measurements of papers 1 and 2 strongly suggest that TKR is "strung out" along field lines both in the region of the plasma sheet and in the dayside cusp.

3) TKR emanates from over a very wide altitude range due to a mechanism whose "efficiency", i.e. occurrence rate and power, varies inversely with altitude.

These general properties - occurrence rate, source location geometry and altitude - must be encompassed into any theory attempting to explain TKR.

#### ACKNOWLEDGEMENTS

We thank our colleagues Drs. Donald Fairfield, Norman Ness, Robert Benson and Paul Rodriguez for helpful discussions. We also thank Ms. S. Vaughan and Ms. P. Harper for their assistance with the data processing.

## REFERENCES

- Alexander, J.K. and M.L. Kaiser, Terrestrial kilometric radiation:  
1 - spatial structure studies, J. Geophys. Res., 81, 5948, 1976.
- Alexander, J.K. and M.L. Kaiser, Terrestrial kilometric radiation:  
2 - emission from the magnetospheric cusp and dayside magnetosheath,  
J. Geophys. Res., 82, 98, 1977.
- Brown, L.W., The galactic radio spectrum between 130 and 2600 kHz,  
Astrophys. J., 180, 359, 1973.
- Dunckel, N., B. Ficklin, L. Roerden, and R.A. Helliwell, Low-frequency  
noise observed in the distant magnetosphere with OGO-1, J. Geophys.  
Res., 75, 1854, 1970.
- Green, J.L., D.A. Gurnett, and S.D. Shawhan, The angular distribution  
of auroral kilometric radiation, J. Geophys. Res., in press, 1977.
- Gurnett, D.A., The earth as a radio source: terrestrial kilometric  
radiation, J. Geophys. Res., 79, 4227, 1974.
- Gurnett, D.A., The earth as a radio source: the nonthermal continuum,  
J. Geophys. Res., 80, 2751, 1975.
- Gurnett, D.A. and L.A. Frank, A region of intense plasma wave turbulence  
on auroral field lines, U. of Iowa report 76-12, 1976.
- Kaiser, M. and R.G. Stone, Earth as an intense planetary radio source:  
similarities to Jupiter and Saturn, Science, 189, 285, 1975.
- Kurth, W.S., M.M. Baumbach, and D.A. Gurnett, Direction finding measure-  
ments of auroral kilometric radiation, J. Geophys. Res., 80,  
2764, 1975.

Mead, G.D. and D.H. Fairfield, Quantitative magnetospheric models derived from spacecraft magnetometer data, J. Geophys. Res., 80, 523, 1975.

Scarf, F.L., A new model for the high-frequency decametric radiation from Jupiter, J. Geophys. Res., 79, 3835, 1974.

Voots, G.R., D.A. Gurnett, and S.-I. Akasofu, Auroral kilometric radiation as an indicator of auroral magnetic disturbances, J. Geophys. Res., in press, 1977.

## FIGURE CAPTIONS

- Figure 1. The flux distribution at 250 kHz during quiet times ( $AE < 75$ ) over the 06-09 hr zone and during disturbed times ( $AE > 200$ ) over the 21-24 hr zone. The probability (in percent) per unit flux interval has been determined by dividing the number of samples in each flux bin by the total number of samples and the size of the bin. The straight lines with their indicated slopes were determined from a least squares fit.
- Figure 2. The median power flux density spectra observed from above  $25 R_E$  by IMP-6 grouped according to sub-satellite local time and the value of the auroral electrojet index ( $AE$ ) at the time of observation. This particular division of the data with respect to  $AE$  results in essentially equal numbers of IMP-6 measurements in each  $AE$  bin. The flux values were adjusted to a constant distance of  $25 R_E$ .
- Figure 3. The distribution of TKR flux with projected radial distance at 292 kHz as measured by RAE-2 from lunar occultations. Panel (a) shows the distribution of median flux as observed from first quarter moon (solid dots) and from all local times (open circles). The bottom three panels show the distance distribution for strong (b), moderate (c), and weak (d) events. The flux appears to decrease more rapidly than  $R^{-2}$ .

Figure 4. a) Example of a simple TKR source located above the nighttime auroral zone. The panel on the right shows the average flux spectrum determined from RAE-2 observations immediately preceding and immediately following a lunar occultation of the earth. The left panel shows the source position deduced from that occultation as projected onto the noon-midnight meridian plane. The coordinate system is the Solar Magnetic (SM) folded such that the +Z direction is the sunlit pole. The field lines are from the Mead-Fairfield (1975) MF73D model.

b) Spectrum of a more complex nighttime event displayed in the same format as Figure 4a.

Figure 5. a) Spectrum of a simple dayside cusp event displayed in the same format as Figure 4.

b) Spectrum of a distant cusp event displayed in the same format as Figure 4.

c) Spectrum of emission from the magnetopause/magnetosheath. This figure is basically similar to Figures 5a and b except the occultation was not complete at the lowest frequencies. The shaded area shows the approximate region of the magnetosphere that was continuously obscured from view during the interval from 0930 to 0940 UT, yet as shown in the flux spectrum on the right, a substantial amount of emission persists below 210 kHz. This emission must have emanated from beyond the lunar limb which would have placed it generally beyond the magnetopause.

Figure 6. - IMP-6 spectral observations illustrating the dynamic complexity of TKR. The upper left-hand panel shows the 0.03 to 2.6 MHz dynamic spectral data (10-min resolution) between 1300 and 2400 UT on August 30, 1972. TKR "storms" are observed between 1300 and 1600 UT and between 1900 and 2200 UT. The period near 2015 UT, which indicated splitting of the TKR band, is shown in highly expanded form (5.1-sec resolution) in the lower left, and in the average flux spectrum is shown on the right.

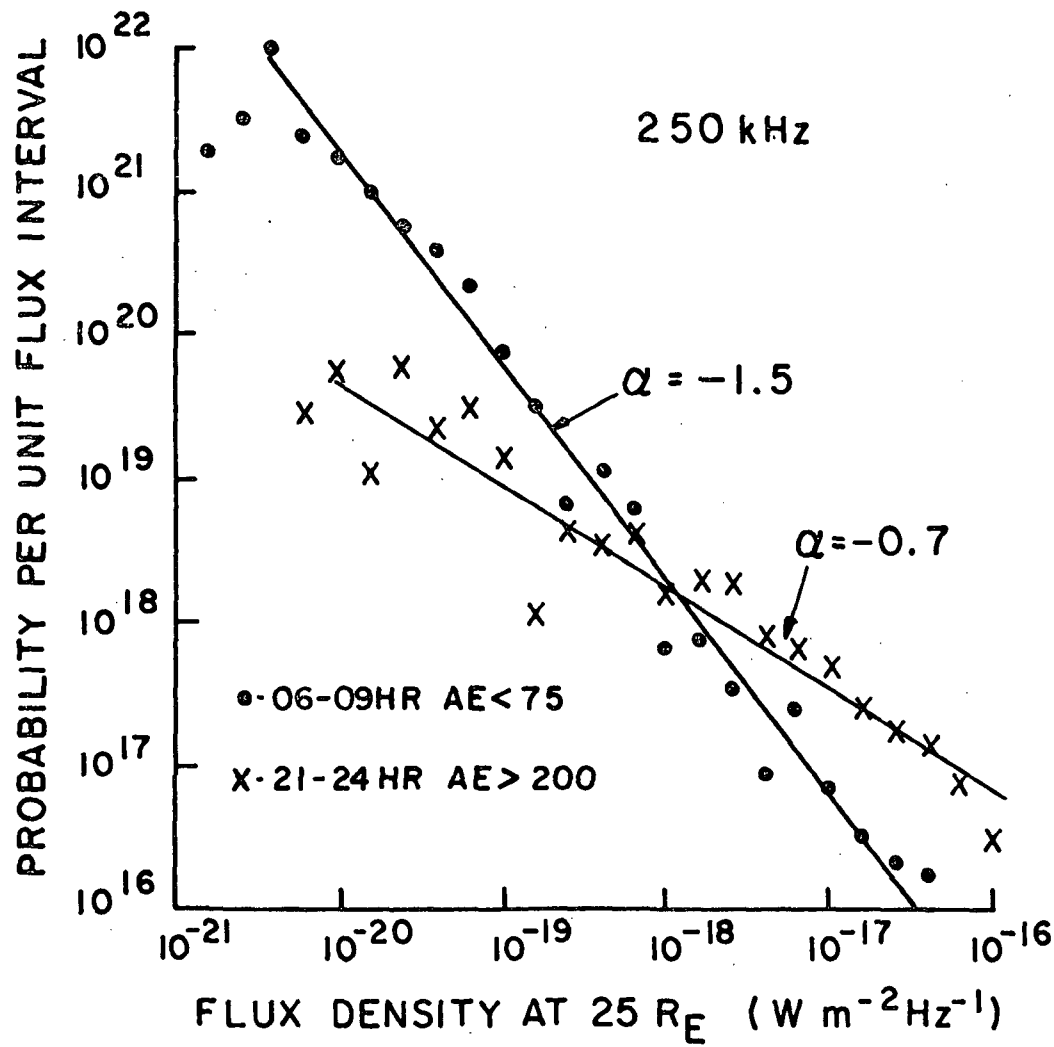
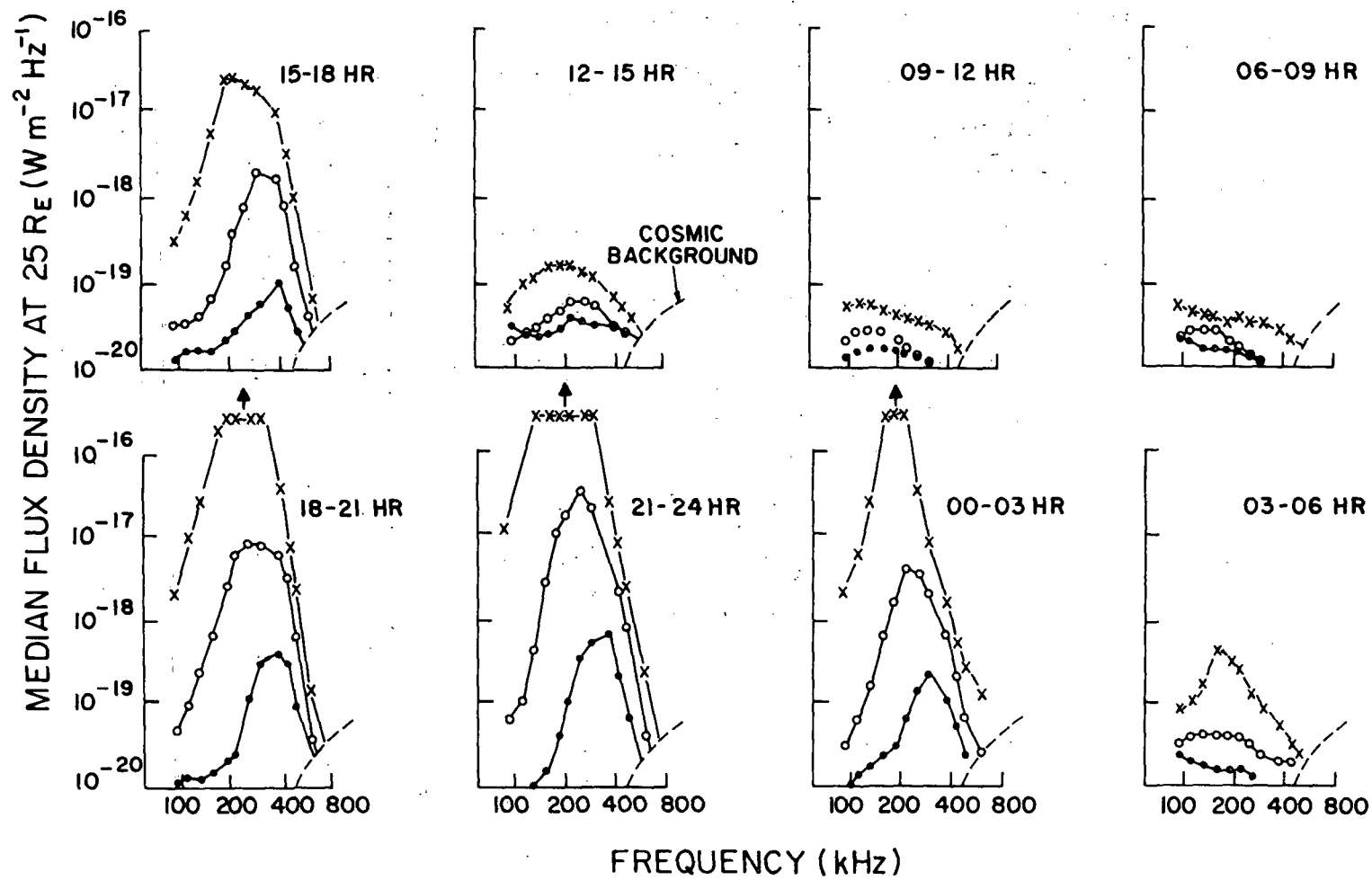


Figure 1



- AE < 75
- 75 < AE < 200
- × AE > 200

Figure 2

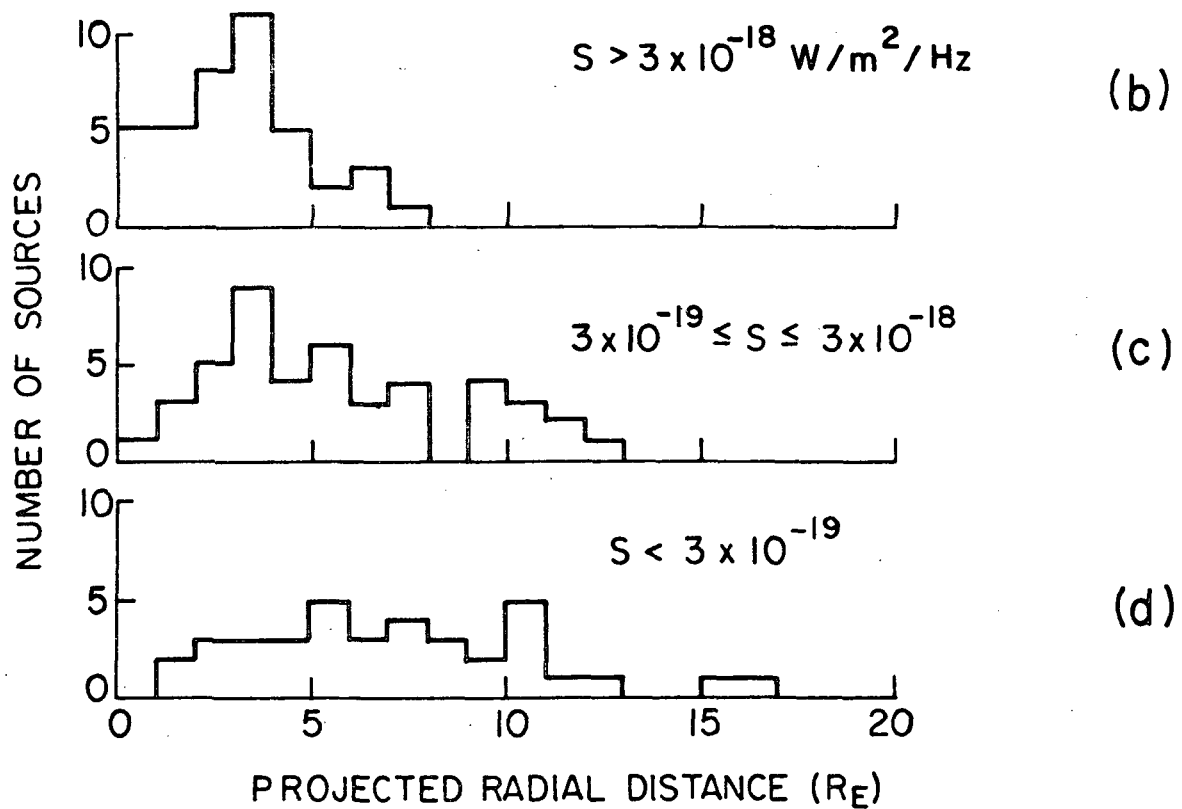
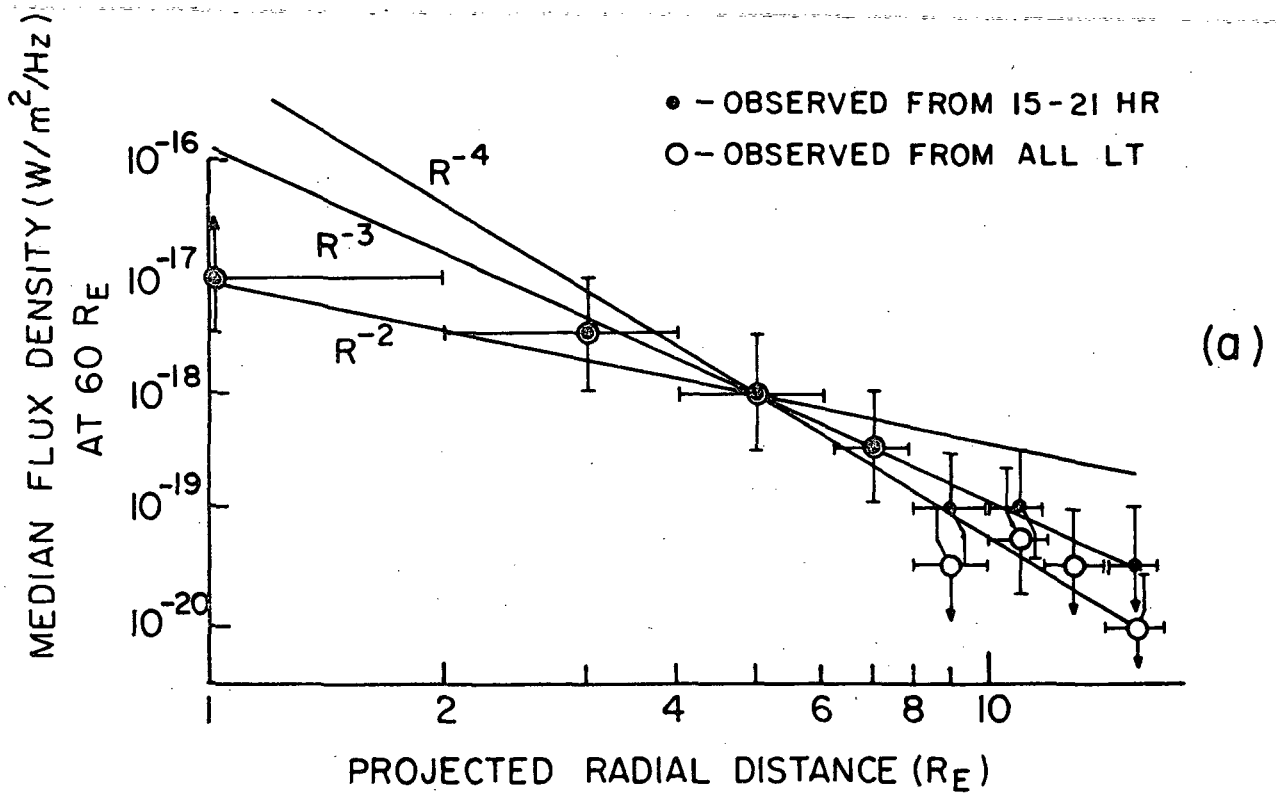
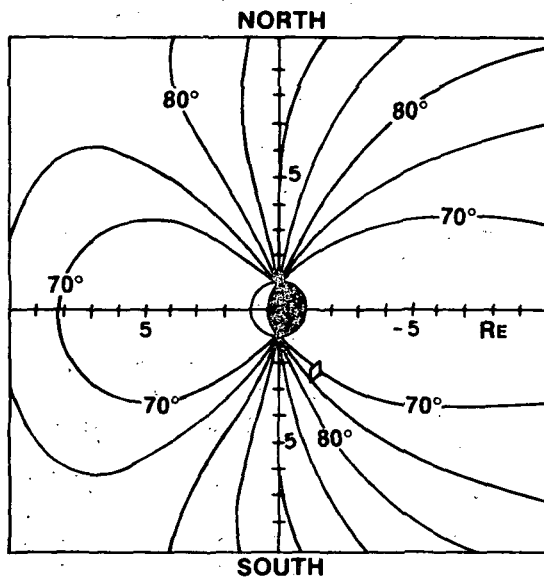


Figure 3



425 KHz SOURCE POSITION

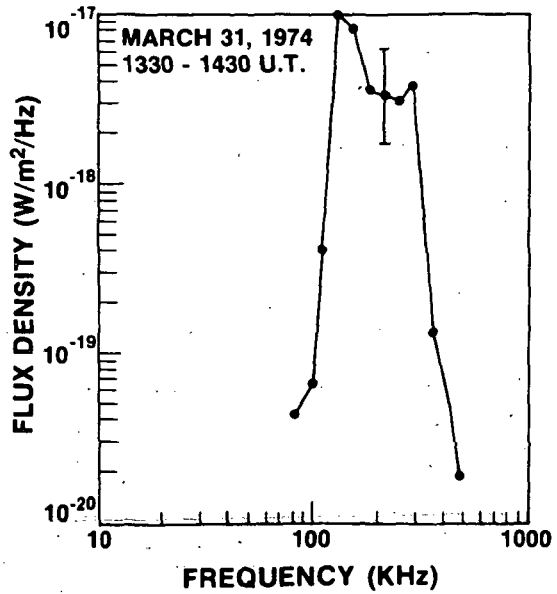
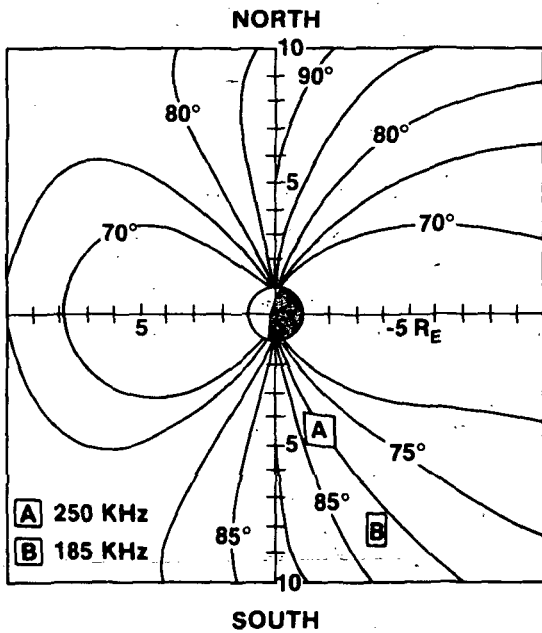
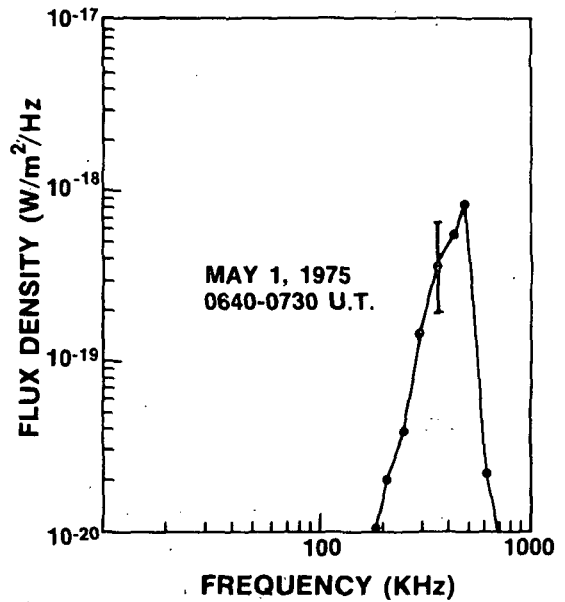
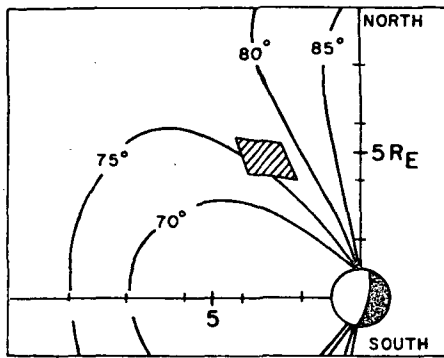
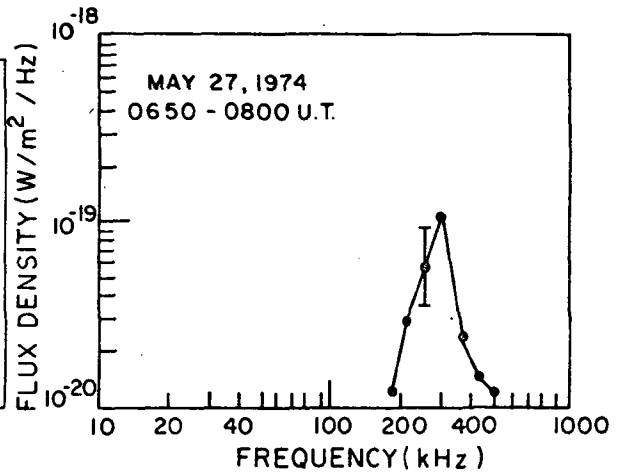


Figure 4

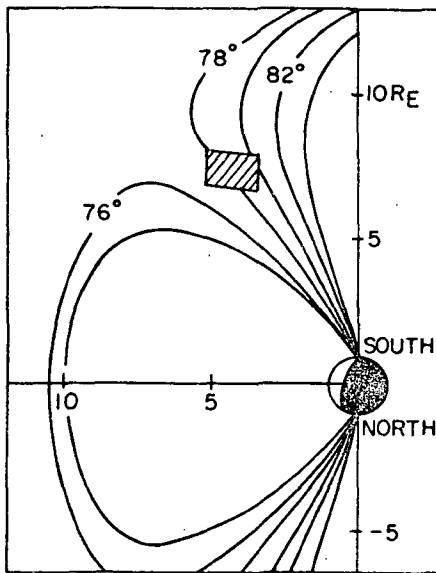
(a)



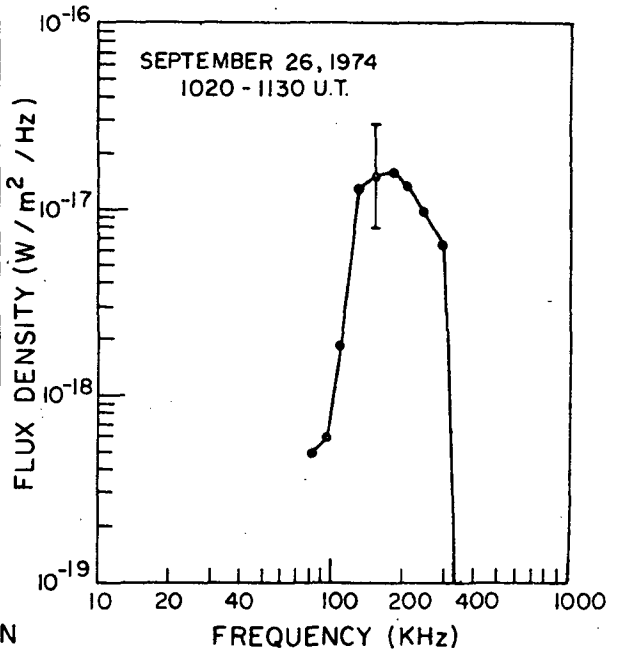
292 KHz OCCULTATION POSITION



(b)



185 KHz OCCULTATION POSITION



(c)

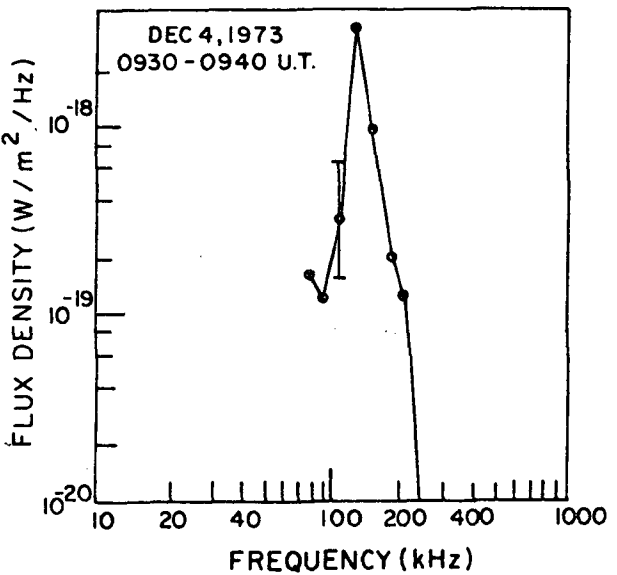
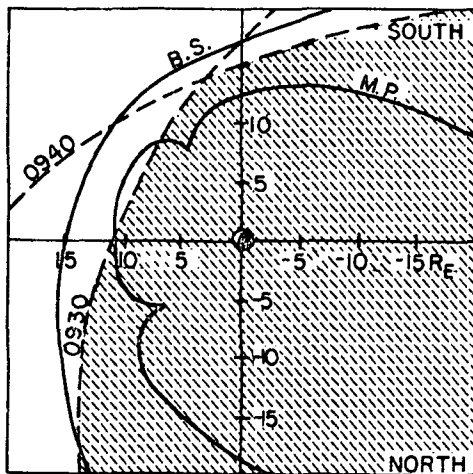


Figure 5

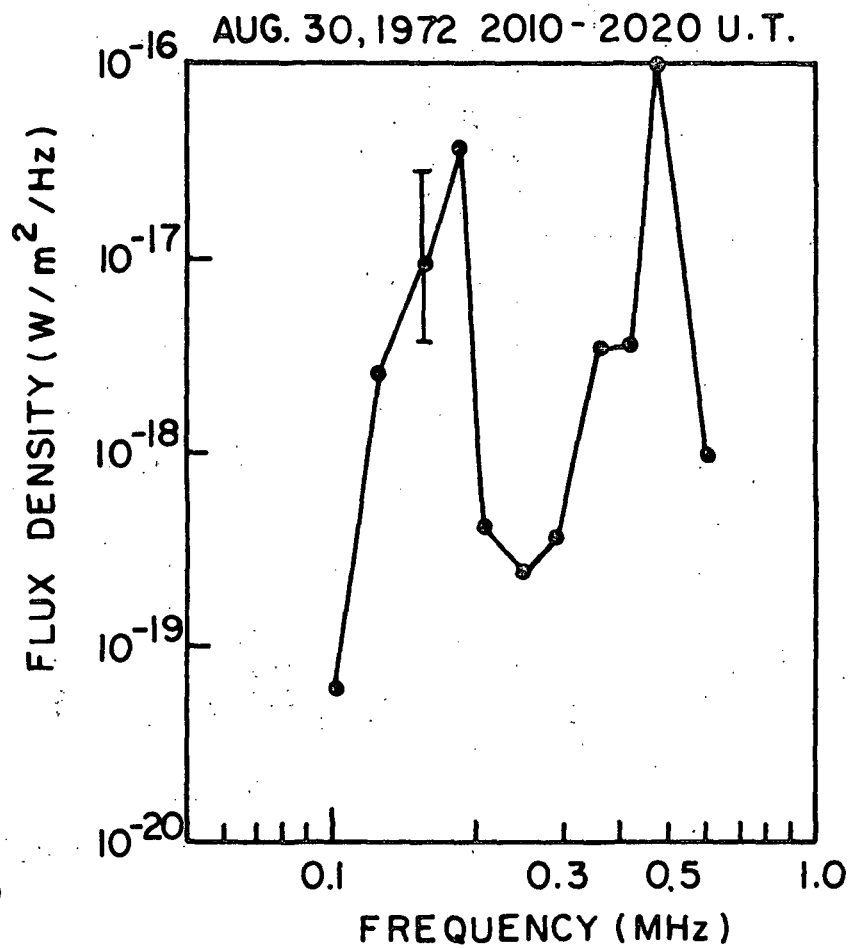
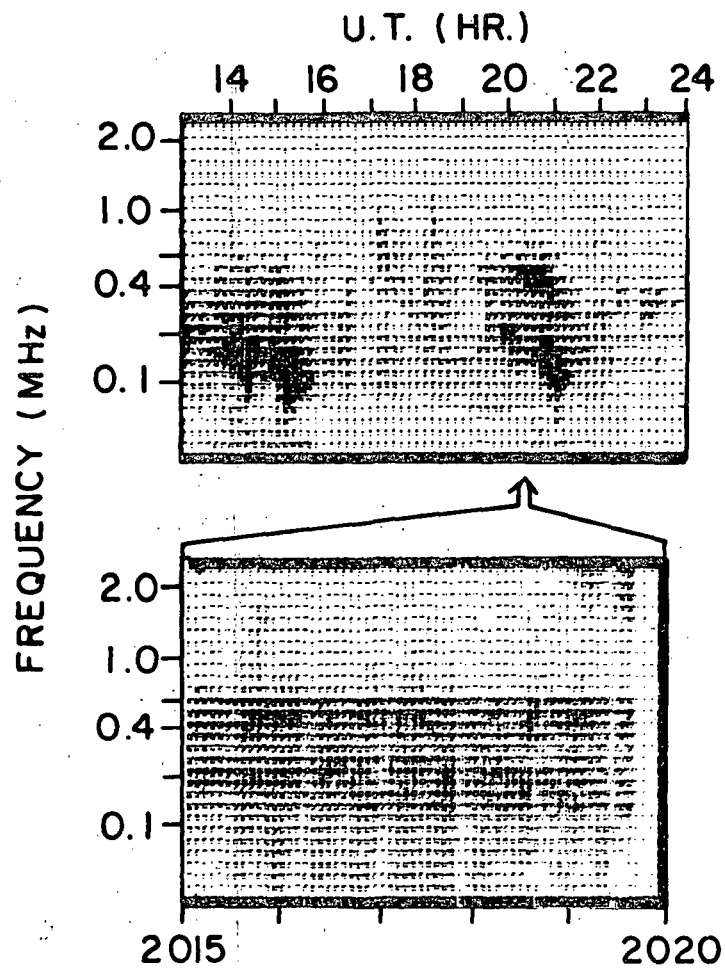


Figure 6